Available online at www.sciencedirect.com
ScienceDirect
Sensors and Actuators B 120 (2006) 187–193
SENSORS AND ACTUATORS B CHEMICAL
www.elsevier.com/locate/snb

Photonic crystal optical biosensor incorporating structured low-index porous dielectric

Ian D. Block [1], Leo L. Chan [1], Brian T. Cunningham *

Nano Sensors Group, University of Illinois at Urbana-Champaign, USA

Received 11 July 2005; received in revised form 20 January 2006; accepted 5 February 2006
Available online 29 March 2006

Abstract

The sensitivity of a photonic crystal optical biosensor is greatly enhanced through the incorporation of low refractive index porous dielectric material into the device structure. In this work, computer models are used to predict the reflectance spectra and sensitivity performance of a one-dimensional photonic crystal biosensor. A manufacturable replication method is demonstrated that can produce a low-index dielectric periodic surface structure with a 550 nm period over large surface areas. The sensitivity of porous glass biosensors is characterized and compared with sensors incorporating non-porous polymer material. Results for detection of proteins, polymer layers, and bulk liquids indicate up to a four-fold sensitivity increase.

Keywords: Optical biosensor; Low-k dielectric; Micro-replication; FDTD; Direct assay; Photonic crystal

1. Introduction

Label-free optical biosensors based upon surface structured photonic crystals have recently been demonstrated as a highly sensitive method for performing a wide variety of biochemical and cell-based assays [1]. The device structure is designed to reflect only a narrow band of wavelengths when illuminated with white light at normal incidence, where positive shifts of the reflected peak wavelength value (PWV) indicate the adsorption of detected material on the sensor surface [2]. By spatially confining incident photons at the resonant wavelength, a high optical field is generated at the sensor surface that extends a short distance into a test sample, much like an evanescent field. The high degree of spatial confinement of resonant photons within the device structure leads to a strong interaction between the structure and adsorbed biomaterial, and to the ability to perform high resolution imaging of protein and cell attachment [3].

Previously, photonic crystal optical biosensors have been fabricated from continuous sheets of plastic film using a process in which the periodic surface structure is replicated from a silicon master wafer using a UV-cured polymer material [4]. This patterned polymer is subsequently coated with a high refractive index TiO_2 layer that is generally thinner than the height of the surface structure. Such devices have been demonstrated for a wide variety of biochemical and cell-based assays, with a mass density sensitivity resolution less than 0.1 pg/mm^2 and a large dynamic range enabling single cell detection [5]. In general, optimization of the device sensitivity requires increasing the interaction of the electromagnetic field intensity distribution with the biological material deposited atop the photonic crystal surface. Therefore, selection of optical materials and design of the surface structure topology should be aimed at extending the electromagnetic field profile from the interior regions of the photonic crystal (where they cannot interact with adsorbed material) to the region adjacent to the photonic crystal that includes the liquid test sample. In this work, we demonstrate that the substitution of an extremely low refractive index material for the surface structure within the photonic crystal biosensor has the desired effect of substantially increasing detection sensitivity.

We used rigorous coupled wave analysis (RCWA) and finite difference time domain (FDTD) simulations to predict the resonant wavelength and bulk refractive index sensitivity of a one-dimensional surface photonic crystal biosensor. The device incorporates a low-index ($n = 1.17$) nanoporous dielectric surface structure in place of the polymer ($n = 1.39$) surface structure

* Corresponding author. Tel.: +1 217 265 6291.
E-mail address: bcunning@uiuc.edu (B.T. Cunningham).
[1] These authors contributed equally to this work.

0925-4005/$ – see front matter © 2006 Elsevier B.V. All rights reserved.
doi:10.1016/j.snb.2006.02.006

reported previously. We use a soft contact embossing method to create a surface-structured low-index porous film on glass substrates with a depth and period that are identical to the previous polymer structures to enable a side-by-side sensitivity comparison. The sensitivity of porous glass biosensors is compared to nonporous polymer biosensors through methods that characterize sensitivity to bulk refractive index and surface-adsorbed material. Finally, a protein binding assay comparison is performed to demonstrate sensor stability and the ability to functionalize the device for selective detection.

2. Materials and methods

2.1. Computer simulation

The polymer and porous glass sensors were modeled and simulated using two software packages. First, a 2-D diffraction grating analysis tool (GSOLVER) employing the RCWA algorithm provides a quick and simple method for initial sensor modeling. Second, FDTD (Lumerical) provides a much more versatile and powerful tool that can calculate any field component at any temporal or spectral location for an arbitrary optical device illuminated by an arbitrary source [6]. FDTD was used to verify RCWA results and to gain deeper insight into the effects of modifying the sensor structure.

2.2. Sensor fabrication

In the proposed device, we incorporate a sol–gel derived low-index nanoporous silica thin-film [7] in place of the UV-cured epoxy used in previous designs. Since the low-index material cures by heat rather than UV exposure, it was necessary to develop a new fabrication process. We desired to retain a low-cost imprinting method, though it was obvious that a plastic substrate could not sustain the requisite high temperatures for porous glass annealing. One possible approach to sol–gel glass imprinting was to use a polydimethylsiloxane (PDMS) mold and a glass substrate [8].

The sub-wavelength grating structure of the low-k biosensor was fabricated using a combination of lithography, molding, and imprinting processes. The process begins with production of a silicon "master" wafer, that is patterned by deep-UV photolithography with a linear grating photoresist pattern of parallel 275 nm width photoresist lines separated by 275 nm width spaces. The photoresist is used as a mask for reactive-ion etching of ~170 nm deep trenches into the silicon wafer. After etching, the photoresist is removed, and the silicon wafer contains a positive image of the surface structure desired in the finished sensor. Sylgard 184 PDMS (Dow) "daughter" molds are then replicated from the silicon master wafer. The liquid PDMS is poured into a rectangular metal frame placed on top of the silicon master wafer and then cured at 90 °C for 24 h. To facilitate release of the cured PDMS mold from the silicon wafer, the wafer was surface treated with a release layer of dimethyldichlorosilane (Repel Silane, Amersham Biosciences) [9]. The PDMS replicas are then used to imprint a thin-film of uncured Nanoglass® (Honeywell Electronic Materials), a low-index sol–gel glass, spun-on

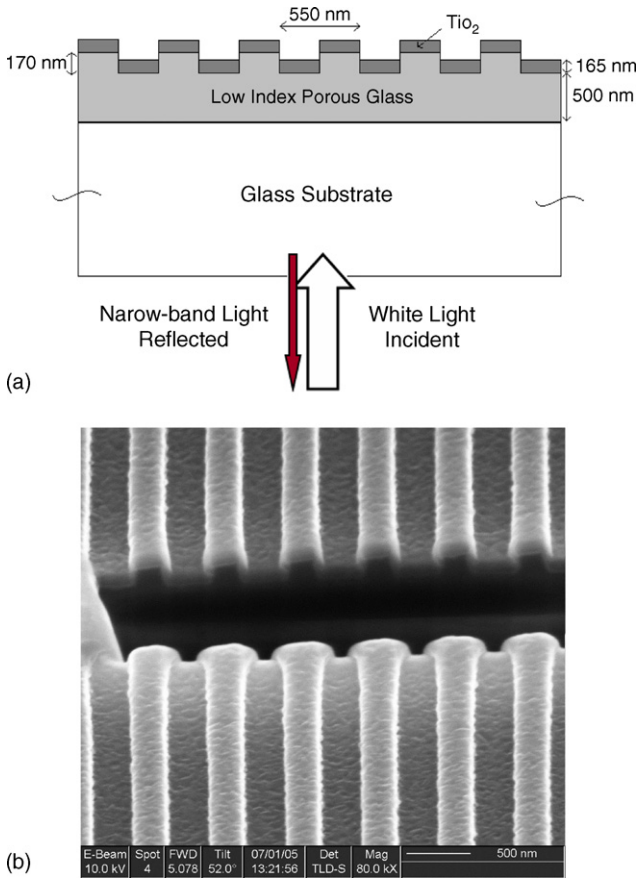

Fig. 1. Cross-section schematic (a) and scanning electron micrograph (SEM) (b) of porous glass photonic crystal sensor. Surface roughness visible in SEM is due to a carbon coating atop the TiO_2 film used to enhance image quality.

to a glass substrate. Once the low-index dielectric becomes rigid, the flexible PDMS mold is removed and the sol–gel glass is fully cured by further baking. The sensor structure is completed by evaporating 165 nm of TiO_2 onto the patterned surface. A subsequent surface treatment with dimethyldichlorosilane encourages bio-adsorption and promotes sensor stability. A schematic illustration and scanning electron micrograph of the device cross-section are shown in Fig. 1(a and b).

The polymer structure is similar to that described in a previous publication [4]. It contains a periodic surface structure of UV-cured polymer that is subsequently overcoated with a layer of TiO_2 deposited by a sputtering process. The polymer periodic surface structure is also formed by a replica molding process, in which an 8-in. diameter silicon "master" wafer is used as a mold. A thin layer of UV-curable polymer is squeezed between a flexible transparent plastic substrate film and the silicon wafer. The polymer is allowed to flow into the silicon mold before it is rapidly cured to a solid by exposure to UV light. After curing, the replica (attached to the plastic film) is peeled away from the silicon mold, so the silicon may be used for additional replicas. Because the same silicon "master" is used to produce the polymer and porous glass devices, both structures have a 550 nm period and 170 nm imprint depth. The grating period and grating depth were verified by scanning electron microscopy. The

two devices will be referred to as the "polymer" and "porous glass" sensors throughout the remainder of this paper. The polymer devices were provided as an array of sensors aligned and attached to bottomless 96-well standard microtiter plates (SRU Biosystems). The porous glass devices are fabricated on 75 mm × 25 mm × 1 mm glass microscope slides. Adhesive rubber wells (Research International Corp.) are attached to the glass surface to provide liquid containment for five to six sensors on each slide.

2.3. Instrumentation

The configuration of the readout instrument has been reported previously [2]. A broad wavelength light source is coupled to an optical fiber that illuminates a ∼2 mm diameter region of the photonic crystal surface from below the substrate at normal incidence. Reflected light is collected by a second optical fiber that is bundled next to the illuminating fiber, and measured by a spectrometer. An automated motion stage enables parallel collection of reflectance data at timed intervals from many wells in order to acquire kinetic information.

2.4. Sensor characterization

2.4.1. Bulk refractive index measurement

Deionized water (DI H_2O, $n = 1.333$) and Isopropyl Alcohol (IPA, $n = 1.378$) are used to determine the bulk shift coefficient of each sensor. First, DI H_2O is pipetted onto the surface of the sensor and the PWV is measured. Next, the surface is thoroughly dried and the previous step is repeated for IPA. The bulk shift coefficient between DI H_2O and IPA can then be calculated as the change in PWV divided by the change in bulk refractive index.

2.4.2. PPL bio-adhesion test

Sensitivity to surface-adsorbed material was characterized by the detection of a single layer film of poly(Lys, Phe) (PPL; Sigma–Aldrich; MW = 35,400 Da) prepared to a 1.0 mg/ml solution with 0.01 M phosphate buffered saline (PBS; pH 7.4) applied to the sensor surface. At a sampling interval of 1 min, the bio-adhesion test commenced with the pipetting of PBS into the test wells. After 10 min, the buffer was replaced with PPL solution and was allowed to stabilize for 30 min. The PPL solution was then removed, and PBS was used to rinse the wells. The rinse solution was removed and subsequently filled with fresh PBS for the final 30 min of data acquisition.

2.4.3. Multilayer polymer test

In order to characterize the differential sensitivity as a function of distance from the sensor surface, a series of polymer electrolyte monolayers were deposited on the sensors. By alternating between positively and negatively charged polymer layers, a stack of uniform, self-limiting polymers may be formed on the sensor while it is continuously monitored on the detection instrument [10]. Three different polyelectrolytes are deposited onto the sensor surface: anionic poly(sodium 4-styrenesulfonate) (PSS; MW = 70,000 Da), cationic poly(ethyleniminie) (PEI; MW = 60,000 Da), and cationic poly(allylamine hydrochloride) (PAH; MW = 70,000 Da). The polyelectrolytes were purchased from Sigma–Aldrich. A 0.9 M NaCl buffer solution (Sigma–Aldrich) is prepared with deionized water. The polyelectrolytes were dissolved in the buffer solution at a concentration of 5 mg/ml. At a 1 min sampling interval, the multilayer surface sensitivity characterization is performed in 5 min steps. First, NaCl buffer was pipetted into the sensor wells. Next, the buffer was removed and replaced by PEI solution. The PEI solution was then removed, and PBS was used to rinse the wells. The rinse solution was removed and subsequently filled with fresh buffer. The previous two steps were repeated for PSS and PAH until seven PSS-PAH layers have been deposited upon the single PEI layer.

2.4.4. Bioassay: protein A—IgG

To demonstrate selective detection by the proposed device, we performed a bioassay that characterizes the affinity of human, sheep and chicken IgG for protein A. Protein A (Pierce Biotechnology) is prepared with 0.01 M PBS to a concentration of 0.5 mg/ml. The buffer is filtered with a 0.22 μm syringe filter (Nalgene) before use. Human, sheep, and chicken immunoglobulin-G (IgG) serums (Sigma–Aldrich) are diluted in 0.01 M PBS to a concentration of 0.5 mg/ml. Allowing 30 min between each step and sampling at a 1 min interval, PBS solution was first pipetted into the sensors wells. Next, the buffer was replaced by protein A solution. The well was then rinsed three times and filled with buffer. After the signal stabilized, the buffer in three of the wells was replaced by human, sheep, or chicken IgG, while the fourth was left as a reference containing only the buffer. Finally, the IgGs were removed and the wells were again rinsed and filled with PBS for the final 30 min of data acquisition.

3. Results

3.1. Computer simulation

RCWA and FDTD simulations both indicated that replacement of the patterned UV-cured polymer of previous devices with a material of lower refractive index would produce a two-fold increase in the bulk shift coefficient. The resonant wavelength of the porous glass sensor immersed in DI H_2O was predicted by RCWA to be 844.3 nm with a full-width at half-maximum (FWHM) of approximately 2 nm, as shown in Fig. 2. Simulation predicts further improvements in the bulk shift coefficient with slight modifications to the sensor geometry.

The bulk sensitivity test using DI H_2O and IPA was performed on 23 porous glass sensors and 11 polymer sensors. The average PWV shifts were 13.6 ± 1.0 and 6.3 ± 1.3 nm for the porous glass and polymer sensors, respectively. The bulk shift coefficient ($\Delta PWV/\Delta n$) of the porous glass sensor is measured to be 2.2 times greater than that of the polymer device. Measurements of the porous glass device in DI H_2O give an average PWV of 829.5 ± 16.5 nm and FWHM of 3.5 ± 2.5 nm. One of the measured spectra is illustrated in Fig. 3, where the response has been normalized to a perfect reflector to account for any instrumenta-

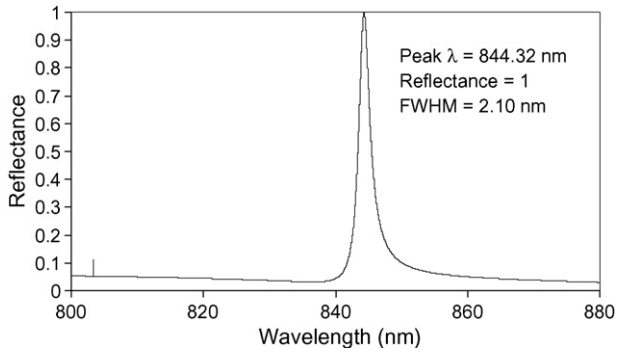

Fig. 2. Resonant peak of porous glass sensor exposed to deionized water, as predicted by RCWA simulation.

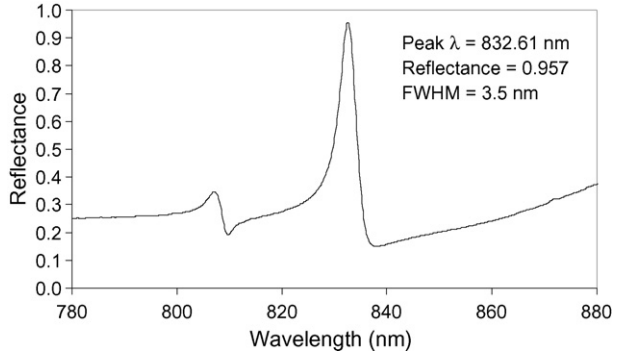

Fig. 3. Experimentally measured resonant peak of porous glass sensor immersed in deionized water.

tion losses. The lower reflection efficiency and broader FWHM measured from the replicated devices can be attributed to small but measurable material losses and to imperfections observed in the replicated structure. The large variability of measured spectral characteristics is due, at least in part, to using several slightly different (though nominally identical) master patterns and to a lack of automation of the replication process.

3.2. PPL bio-adhesion test

PPL was deposited on five porous glass and nine polymer sensors. Fig. 4 compares the kinetic plots of each device, showing a ∼4× increase in surface sensitivity for the porous glass sensor. The first step establishes a baseline, the second corresponds to the rapid surface adsorption and saturation of PPL, and the final third of the curve illustrates the monolayer stability after eliminating weakly bound molecules by rinsing with PBS buffer. The lack of data around 45 min corresponds to the time necessary to rinse all of the wells. The PWV shifts generated during PPL immobilization onto the porous glass sensor saturate more slowly than that measured using the polymer devices. Clearly, the porous glass sensor surface is significantly less conducive to protein monolayer adsorption. The authors anticipate that further surface chemistry optimization should mitigate this effect. Nonetheless, the porous glass sensor exhibits excellent stability after unbound molecules are washed away.

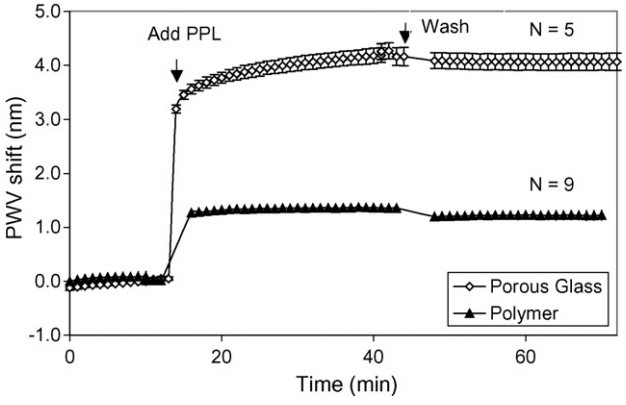

Fig. 4. Kinetic plot comparing PWV shifts for PPL deposited onto both sensor designs.

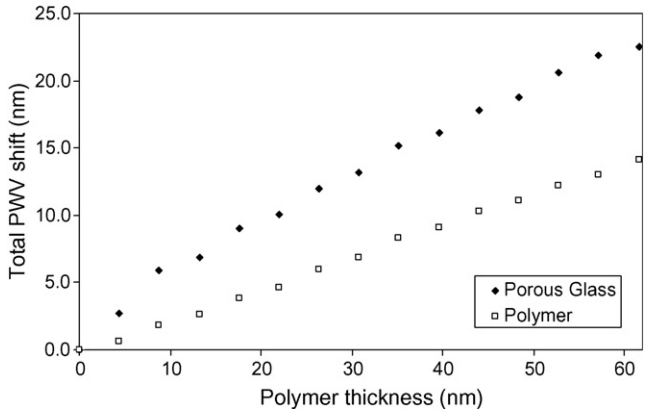

Fig. 5. Spatial profile of PWV shift versus polymer thickness, where alternating layers of PSS and PAH contribute to the total measured shift.

3.3. Multilayer polymer test

The 14 alternating layers of PSS and PAH described previously each cause a measurable shift in the detected PWV as they are adsorbed onto the surface. Fig. 5 gives a spatial profile of PWV shift versus polymer thickness, where each PWV shift was measured in buffer after the wash step. Each monolayer of polyelectrolyte is approximately 4.4 nm thick and has a refractive index of 1.49 [11]. The porous glass sensor exhibits an average surface sensitivity ∼1.5× that of the polymer sensor. However, note that each of the first two layers (∼9 nm) deposited onto the porous glass device cause a PWV shift with twice the magnitude of each of the remaining layers, while no such effect is observed for the polymer device.

3.4. Bioassay: protein A—IgG

Protein A was introduced into 15 porous glass and 16 polymer sensor wells. The resulting PWV shift after the wash step was ∼4× greater for the porous glass devices, as shown in Fig. 6. As in the case of the PPL monolayer adsorption, the lower PWV shift after rinsing (at $t \sim 65$ min, where there is a gap in the data during the rinsing process) is due to elimination of weakly bound Protein A molecules. Fig. 7 illustrates the measured binding kinetics of human, sheep and chicken IgG with protein A for

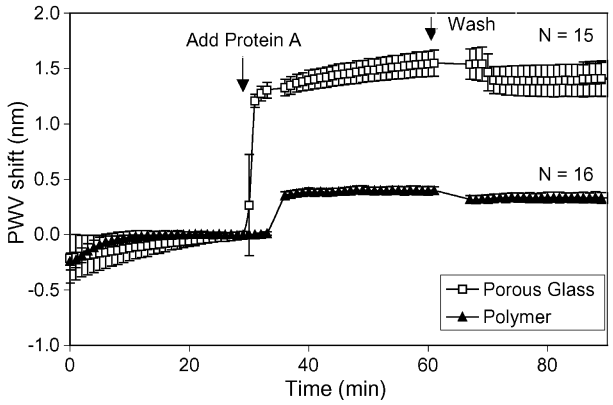

Fig. 6. Kinetic plot comparing PWV shifts for protein A deposited onto both sensor designs.

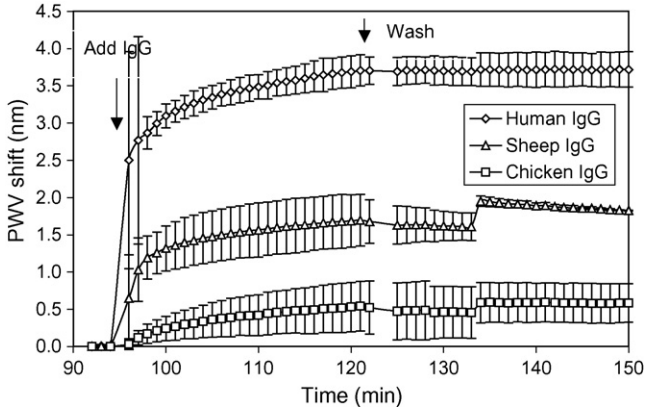

Fig. 7. Binding kinetics of three animal IgGs to protein A measured with the porous glass biosensor.

the porous glass sensor, while Fig. 8 gives an endpoint PWV shift comparison (relative to a reference well without IgG) between the two devices for each antibody. Protein A surface adsorption saturated much more quickly on the polymer sensor surface, similar to that observed in the PPL bio-adhesion test. The porous glass device exhibits increasingly greater sensitivity for antibodies with higher affinity for protein A. Human IgG binding is detected with twice the sensitivity, while chicken IgG, lacking any specificity for protein A, results in an equivalent response,

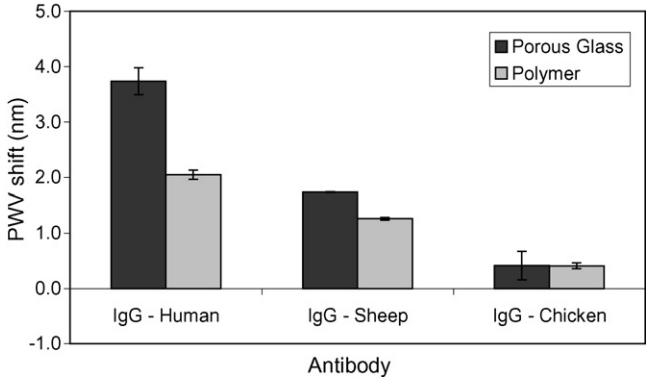

Fig. 8. Sensor comparison of PWV shifts for each of the different IgG—protein A interactions.

and provides a measure of non-specific binding [12]. Error bars for performing the same assay with multiple sensors were found to be smaller for the polymer sensors, which are produced in a manufacturing environment. The porous sensors were produced by hand in a laboratory environment, and are thus less reproducible from one device to another.

4. Discussion

The photonic crystal biosensor is designed to couple electromagnetic energy to biological material deposited upon its surface from a liquid test sample. While the device itself consists of a low refractive index surface structure and a high refractive index dielectric coating, the liquid test sample that fills in the surface structure must also be considered an integral part of the sensor—and the only dynamic component that can induce a change of resonant wavelength. The motivation for incorporating an extremely low refractive index material into the photonic crystal biosensor structure is to spatially bias the electromagnetic field of the resonant wavelength toward the liquid test sample and away from the interior regions of the photonic crystal that do not interact with surface adsorbed material. Through the use of a nanoporous material with a refractive index less than that of water, the desired sensitivity improvement has been achieved.

The materials and methods described in this paper should lend themselves to a manufacturable fabrication process. The use of spin-on low-k dielectric materials leverages off the large investments made in the integrated circuit manufacturing community, who require rapid processing, structural stability, and exclusion of liquid penetration. A unique aspect of this work is the use of an imprinting method to accurately impart a submicron surface structure to a nanoporous glass film without the use of photolithography. The presence of the imprint tool on the surface of the low-k film during the initial stage of the curing process did not alter the refractive index of the final cured structured film. The imprinting method enables substantial cost to be incurred only in the production of the "master" silicon wafer, which is in turn used to produce a nearly unlimited number of "daughter" PDMS imprinting tools. Each PDMS tool can be used to produce a large number of sensor structures without damage to the tool because little force is needed to make the spun-on liquid low-k layer conform to the tool. After imprinting, the low-k dielectric film is cured rapidly on hotplates, using methods that are easily automated. The use of a flexible imprinting tool was found to be advantageous over imprinting from the silicon master wafer directly, as the PDMS mold was easier to release from the partially cured low-k film, and was capable of allowing permeation of volatile solvent released during the cure process. Although only 1 in. × 3 in. microscope slide regions were imprinted in the work shown here, the imprinting method can be scaled to larger surface areas to enable production of sensor areas large enough to cover an entire 96- or 384-well standard microplate (approximately 3 in. × 5 in.). Characterization of sensors produced in these formats will be the topic of a future publication.

It should be noted that our RCWA simulations predict a higher PWV and slightly lower bulk shift coefficient than that measured experimentally for the porous glass devices. However, predicted

and measured values for the polymer sensors are in much better agreement. This discrepancy can be attributed to the different TiO_2 coating processes used for the two device designs. The polymer sensors use a sputtering process that has been verified to deposit films with a refractive index equal to that value used in the simulations ($n = 2.25$). This same value was used to predict porous glass biosensor performance. However, the refractive index of the films evaporated onto the porous glass devices were measured to be considerably lower than that utilized in the simulation model ($n = 1.86$). If an appropriate adjustment is made to the computer model, significantly better agreement between simulation and experiment is obtained.

An interesting and useful result found during comparison of porous glass sensor structures with polymer sensor structures is the disparity in sensitivity gains between bulk refractive index sensitivity and surface-adsorbed layer sensitivity. While computer models accurately predict the $\sim 2\times$ sensitivity increase measured for PWV shift induced by a bulk refractive index change of the solution covering the porous glass sensor surface, a $\sim 4\times$ increase of PWV shift was consistently measured for thin layers of adsorbed material. By measuring the PWV shift as a function of thickness using the polymer multilayer experiment (Fig. 5), we are able to characterize the strength of interaction of the coupled electromagnetic field as a function of distance away from the sensor surface. We find that, for the porous glass sensors, the interaction is particularly strong for the first few monolayers of adsorbed polymer, while the relationship between polymer thickness and PWV is highly linear for each adsorbed monolayer on the polymer sensor structure. The interaction between the test sample and the resonant electromagnetic field distribution is highly complex, as detected material can adsorb to the horizontal and vertical surfaces of the structure, where a characteristic field profile extends into the sample from each surface. While future work will entail a more detailed characterization of the field profile by FDTD simulation, the present work clearly shows that surface-based detection sensitivity is enhanced beyond the improvements in bulk sensitivity for the porous glass biosensor. Because the majority of biomolecular interactions are expected to occur within the first few nanometers from the sensor surface, the surface sensitivity is of greatest importance for increasing sensitivity in the context of surface-based biochemical assays.

5. Conclusion

We have demonstrated a novel photonic crystal biosensor incorporating a surface-patterned low-index material that exhibits up to a four-fold sensitivity increase over similar sensors that use a patterned higher-index polymer. Computer simulations provided accurate predictions of the porous glass sensor behavior. Several experiments explored differing measures of sensitivity by introducing a bulk index change, generating both a single protein monolayer as well a multilayer polymer stack, and performing a simple affinity bioassay. The comparative antibody–antigen assay demonstrated the ability of the biosensor to sustain stabile biomolecular monolayers and to predict relative binding affinities. The increased sensitivity of the porous glass device will enable more accurate characterization of smaller molecules at lower concentrations.

Acknowledgements

This material is based upon work supported by the National Science Foundation under Grant No. 0427657. Any opinions, findings, and conclusions or recommendations expressed in this material are those of the author(s) and do not necessarily reflect the views of the National Science Foundation. The authors gratefully acknowledge SRU Biosystems for providing financial support for this work and Honeywell Electronic Materials for the donation of Nanoglass® low-k porous dielectric material. The authors also extend their gratitude to the support staff of the Micro and Nanotechnology Laboratory at the University of Illinois at Urbana-Champaign.

References

[1] B.T. Cunningham, P. Li, S. Schulz, B. Lin, C. Baird, J. Gerstenmaier, C. Genick, F. Wang, E. Fine, L. Laing, Label-free assays on the BIND system, J. Biomol. Screen. 9 (2004) 481–490.
[2] B.T. Cunningham, P. Li, B. Lin, J. Pepper, Colorimetric resonant reflection as a direct biochemical assay technique, Sens. Actuators B Chem. 81 (2002) 316–328.
[3] P. Li, B. Lin, J. Gerstenmaier, B.T. Cunningham, A new method for label-free imaging of biomolecular interactions, Sen. Actuators B Chem. 99 (2004) 6–13.
[4] B.T. Cunningham, J. Qiu, P. Li, J. Pepper, B. Hugh, A plastic colorimetric resonant optical biosensor for multiparallel detection of label-free biochemical interactions, Sens. Actuators B Chem. 85 (2002) 219–226.
[5] B. Lin, P. Li, B.T. Cunningham, A label-free biosensor-based cell attachment assay for characterization of cell surface molecules, Sens. Actuators B Chem., in press.
[6] K.S. Kunz, R.J. Luebbers, The Finite Difference Time Domain Method for Electromagnetics, CRC Press, Boca Raton, 1993.
[7] D.M. Smith, Simplified process for producing nanoporous silica, Patent No. 6,395,651, Morristown, NJ, 2002.
[8] V.K. Parashar, A. Sayah, M. Pfeffer, F. Schoch, J. Gobrecht, M.A.M. Gijs, Nano-replication of diffractive optical elements in sol–gel derived glasses, Microelectron. Eng. 67-8 (2003) 710–719.
[9] M. Beck, M. Graczyk, I. Maximov, E.L. Sarwe, T.G.I. Ling, M. Keil, L. Montelius, Improving stamps for 10 nm level wafer scale nanoimprint lithography, Microelectron. Eng. 61-2 (2002) 441–448.
[10] B.T. Cunningham, J. Qiu, P. Li, C. Baird, Enhancing the surface sensitivity of colorimetric resonant optical biosensors, Sens. Actuators B Chem. 87 (2002) 365–370.
[11] C. Picart, G. Ladam, B. Senger, J.-C. Voegel, P. Schaaf, F.J.G. Cuisinier, C. Gergely, Determination of structural parameters characterizing thin films by optical methods: a comparison between scanning angle reflectometry and optical waveguide lightmode spectroscopy, J. Chem. Phys. 115 (2001) 1086–1094.
[12] D.D. Richman, P.H. Cleveland, M.N. Oxman, K.M. Johnson, The binding of Staphylococci protein A by the sera of different animal species, J. Immunol. 128 (1982) 2300–2305.

Biographies

Ian D. Block received a BS in Electrical & Computer Engineering from Cornell University in 2004, and a MS in Electrical Engineering from the University of Illinois at Urbana-Champaign in 2005. He is currently working towards a PhD under the direction of Dr. Brian Cunningham at the University of Illinois. The focus of his research is the design and characterization of enhanced sensitivity photonic crystal biosensors.

Leo Li-Ying Chan is a graduate research assistant at the University of Illinois at Urbana-Champaign in the Nano Sensors Group directed by Dr. Brian T. Cunningham. His research focuses on the characterization of photonic crystal optical biosensors and the optimization of small molecule biodetection using this platform. Before joining Dr. Cunningham's group, Leo Chan served as an undergraduate research at Keck Graduate Institute: Claremont, California, where he worked on the application of free solution electrophoresis to DNA finger printing. He earned his BS and MS in Electrical and Computer Engineering with a minor in Biomedical Engineering from the University of Illinois at Urbana-Champaign, where he is currently pursuing a PhD.

Brian T. Cunningham (PhD) is an Associate Professor of Electrical and Computer Engineering at the University of Illinois at Urbana-Champaign, where he is the director of the Nano Sensors Group. His group focuses on the development of photonic crystal-based transducers, plastic-based fabrication methods, and novel instrumentation approaches for label-free biodetection. Prof. Cunningham is a founder and the Chief Technical Officer of SRU Biosystems (Woburn, MA), a life science tools company that provides high sensitivity plastic-based optical biosensors, instrumentation, and software to the pharmaceutical, academic research, genomics, and proteomics communities. Prior to founding SRU Biosystems in June, 2000, Dr. Cunningham was the Manager of Biomedical Technology at Draper Laboratory (Cambridge, MA), where he directed R&D projects aimed at utilizing defense-related technical capabilities for medical applications. In addition, Dr. Cunningham served as Group Leader for MEMS Sensors at Draper Laboratory, where he directed a group performing applied research on microfabricated inertial sensors, acoustic sensors, optical switches, microfluidics, tissue engineering, and biosensors. Concurrently, he was an Associate Director of the Center for Innovative Minimally Invasive Therapy (CIMIT), a Boston-area medical technology consortium, where he led the Advanced Technology Team on Microsensors. Before working at Draper Laboratory, Dr. Cunningham spent 5 years at the Raytheon Electronic Systems Division developing advanced infrared imaging array technology for defense and commercial applications. Dr. Cunningham earned his BS, MS, and PhD degrees in Electrical and Computer Engineering at the University of Illinois. His thesis research was in the field of optoelectronics and compound semiconductor material science, where he contributed to the development of crystal growth techniques that are now widely used for manufacturing solid state lasers, and high frequency amplifiers for wireless communication.